AIMS Materials Science, 7(2): 160–169.
DOI: 10.3934/matersci.2020.2.160
Received: 16 February 2020
Accepted: 20 April 2020
Published: 23 April 2020

http://www.aimspress.com/journal/Materials

Research article

Structural and multiferroic properties of (Sm, Mn) co-doped $BiFeO_3$ materials

Dao Viet Thang[1,2,*], Nguyen Manh Hung[1,2], Nguyen Cao Khang[2] and Le Thi Mai Oanh[2]

[1] Departement of Physics, Hanoi University of Mining and Geology, 18 Vien Street, Duc Thang Ward, North Tuliem District, Hanoi, Vietnam
[2] Center for Nano Science and Technology, Hanoi National University of Education, 136 Xuan Thuy Road, Cau Giay District, Hanoi, Vietnam

* **Correspondence:** Email: daovietthang@humg.edu.vn; Tel: +84985811377.

Abstract: Pure $BiFeO_3$ (BFO) and (Sm, Mn) co-doped materials were synthesized by the citrate method. Effects of (Sm, Mn) co-doping on the structural, magnetic, electrical and ferroelectric properties of the BFO materials were characterized and investigated by different techniques, such as X-ray diffraction (XRD), Raman scattering spectroscopy, magnetic hysteresis (*M–H*) loops, electric polarization hysteresis loops, and complex impedance spectra measurements. Analysis results of the XRD measurement show that all samples were crystallized in the rhombohedral structure with R_{3C} space group and crystal lattice parameters of a = 0.5584 nm, c = 1.3874 nm and the average crystal size of L_{XRD} = 60 nm for BFO sample. The crystal lattice parameters a, c and the average crystal size L_{XRD} of (Sm, Mn) co-doped samples were found to decrease with the increasing Sm concentration. The Raman scattering spectral show that the position of peaks characteristic for the Fe–O bonds in the (Sm, Mn) co-doped samples shifts toward lower frequency compared to that of BFO. For the (Sm, Mn) co-doped samples, the position of peaks characteristic for Bi–O covalent bonds shifts toward higher frequencies when the Sm concentration increases, confirming that Sm^{3+} and Mn^{2+} ions are substituted into Bi-sites and Fe-sites, respectively. The data from the magnetic hysteresis loop measurements indicate that all samples exhibit weak ferromagnetic behavior. The BFO sample presents weak ferromagnetic properties with a saturation magnetization of Ms = 0.015 emu/g and the remnant magnetization of Mr = 0.007 emu/g. Ferromagnetic properties of the (Sm, Mn) co-doped samples are found enhanced compared to those of BFO. The origin of ferromagnetism of the materials has been considered.

Keywords: X-ray, Raman, (Sm, Mn) co-doped, ferromagnetic, ferroelectric

1. Introduction

Multiferroic materials are known from several previous studies to contain coexisting ferromagnetic (antiferromagnetic), ferroelectric orders and to exhibit ferroelasticity and magnetoelectric (ME) effect in the same structure phase [1–4]. These materials have found broad application in electronic devices, such as information storage, memory sensor, and also in ultrasonic technologies. Due to the competition between the ferromagnetic and the ferroelectric orders, the multiferroic materials are very rarely available in the nature. $BiFeO_3$ (BFO) has a small saturated magnetization and a small electric polarization, that limit the applicability of this materials. This problem can be solved by modification of the magnetic and electrical properties substitution of rare earth ions (such as Sm^{3+}, Nd^{3+}, Gd^{3+}, Ho^{3+}, etc.) into the Bi-sites [5–7] or transition metal ions (such as Ni^{2+}, Co^{2+}, Mn^{2+}, etc.) into the Fe-sites [8–10]. Recently, some studies showed that both the ferromagnetic and ferroelectric properties are enhanced as rare earth (*RE*) and transition metal (*TM*) ions are co-doped into the BFO host materials [11–13]. Chakrabarti et al. [14] and Zhang et al. [15] pointed out that the magnetization of (Eu, Co) or (La, Co) co-doped BFO was enhanced by a few times of that the parent BFO compound. Ye et al. [16] also have shown that the (Ho, Mn) co-doped BFO compound exhibit to improve ferromagnetic and ferroelectric properties compared to those of BFO.

In this work, Sm and Mn are chosen for co-doping into the BFO host materials. Because Sm-doped $BiFeO_3$ can improve magnetic and dielectric properties, Mn substitution for the Fe-site is expected to further affect the magnetic and ferroelectric properties to a greater extent resulting in a larger ME effect at room temperature [16–18]. Some previous studies also have shown that the Mn concentration of about 2% to 3% molar was the appropriate one for effectively doping into the BFO host materials [12,19,20]. In this work, we use a fixed Mn concentration of 3% molar and a Sm concentration in the range from 2% to 12% molar to study the effect (Sm, Mn) co-doping on the structural and other physical properties of BFO.

2. Materials and methods

2.1. Materials synthesis

Pure $BiFeO_3$ and (Sm, Mn) co-doped $BiFeO_3$ materials were synthesized by citrate method. The firstly, $Bi(NO_3)_3{\cdot}5H_2O$, $Fe(NO_3)_3{\cdot}9H_2O$, $Sm(NO_3){\cdot}6H_2O$, and $Mn(NO_3)_2{\cdot}4H_2O$ were dissolved in 35 mL citric acid solution. The solution was then mixed by magnetic stirring at the temperature of 60 °C for 45 min to obtain so solution. Then, temperature of the sol was increased to 100 °C to evaporate the water for 3 h obtaining the wet gel. In the next, the gel was dried at 130 °C for 4 h. Finally, dry gel was annealed at temperature 800 °C for 7 h in air to obtain the powder materials. The chemicals used were: $Bi(NO_3)_3{\cdot}5H_2O$ (Sigma-Aldrich, 98%), $Fe(NO_3)_3{\cdot}9H_2O$ (Sigma-Aldrich, 98%), $Sm(NO_3)_3{\cdot}6H_2O$ (Sigma-Aldrich, 99.99%), $Mn(NO_3)_2{\cdot}4H_2O$ (Sigma-Aldrich, 98%), $C_2H_6O_2$ (Sigma-Aldrich, 98%), and $HOC(COOH)(CH_2COOH)_2$ (Sigma-Aldrich, 99%).

For the measurements of the complex impedance and electric polarization hysteresis loops of all samples, powder materials were compressed at a pressure of 20 MPa into pellets of 6.10^6 nm in diameter and 10^6 nm in thickness. The pellets were sintered at of 800 °C for 5 h. Then, the ceramic pellets were polished to the accurate thickness. Finally, the samples were evenly covered with Pt glue as electrode and sintered at of 500 °C for 3 h to obtain the appropriate specimens for the measurements of complex impedance spectra.

2.2. Microstructural characterization

The microstructure, magnetic and ferroelectric properties of all samples were investigated by using X-ray diffraction (D8 Advance, Cu-K_α radiation), Raman scattering (LabRAM HR Evolution, λ = 532 nm), magnetization hysteresis loops (Lake Shore Cryotronics, 704 VSM), and electric polarization hysteresis loops (Radiant, Precision LC 10 V), and complex impedance measurement (LeCroy equiment with frequency range from 10 Hz to 5.3 MHz and using the LabView 8.0 software).

3. Results and discussion

3.1. X-ray diffraction

The phase formation and crystal structure of $BiFeO_3$ (BFO) and (Sm, Mn) co-doped $BiFeO_3$ materials were investigated by X-ray diffraction (XRD). The XRD patterns of all samples are shown in Figure 1. The refinement of these patterns following the standard cards JPCDS No. 71-2494 revealed that all samples exhibit rhombohedral crystal structure of the original $BiFeO_3$ compound. The main diffraction peaks could be indexed to the (012), (104), (110), (006), (202), (024), (116), (122), (018), and (300) crystalline planes, as indicated in Figure 1a. The XRD patterns of (Sm, Mn) co-doped samples show that Sm^{3+} and Mn^{2+} ions are well incorporated into the BFO crystal lattice. Figure 1b shows a comparison of the positions of the (012), (104) and (110) peaks, which may depict the effects of (Sm, Mn) co-doping on the crystal structure of BFO. As it is seen, the corresponding peaks of the (Sm, Mn) co-doped samples shift toward higher 2θ values compared to those of the undoped BFO sample. From data of XRD analysis, the crystal lattice parameter and the average crystallite size (L_{XRD}) have been determined by using the UnitCell software and the Debye Scherrer's formula, and results are shown in Table 1. As seen in Table 1, the BFO sample has crystal lattice parameters of a = 0.5584 nm, c = 1.3875 nm and the average crystal size L_{XRD} = 60 nm. It is also seen that the crystal lattice parameters and the average crystal size of the (Sm, Mn) co-doped samples decrease when the Sm-concentration increases. This observation can be easily understood considering the large ionic radius of Mn^{2+} (0.067 nm) compared to that of Fe^{3+} (0.065 nm). When the Mn^{2+} ions are substituted into Fe-sites they cause an expansion of the crystal lattice, which in turn increases the length of the Fe/Mn–O bonds. For the (Sm, Mn) co-doped samples, the diffraction peaks shift toward higher 2θ values compare to those of the BFO sample, which could be explained as due to the smaller ionic radius of Sm^{3+} (0.108 nm) compare to that of Bi^{3+} (0.117 nm). The presence of the small Sm^{3+} ions leads to the contraction of the crystal lattice. Furthermore, the Sm^{3+} ion with the small ionic radius is not large enough to fill the 12-sided cavity created by the BO_6 octahedron causing the BO_6 octahedron to rotate (B-site is Fe or Mn), which reduces the 12-sided

cavity volume. So, at the low concentration of Sm ($x \leq 0.08$), the value of a lattice parameter seems to remain unchanged while the value of c slightly decreases to compared with that of BFO sample. For the (Sm, Mn) co-doped samples with higher Sm-concentrations, the rotation BO_6 octahedron is significant leading to the significant reduction of both the a and c parameters. So, the simultaneous substitution of Sm^{3+} and Mn^{2+}, respectively, into the Bi-sites and the Fe-sites leads to the shrank of the crystal lattice, which is related to the decrease of the Bi/Sm–O bonds. This may be the reasons for the decrease of the crystal lattice parameters and the average crystal size, as shown in Table 1. Previous studies also indicated that the lattice parameters change due to the fact that ionic radius of Sm^{3+} is smaller than that of Bi^{3+} and the ionic radius of Mn^{2+} is larger than that of Fe^{3+} [21].

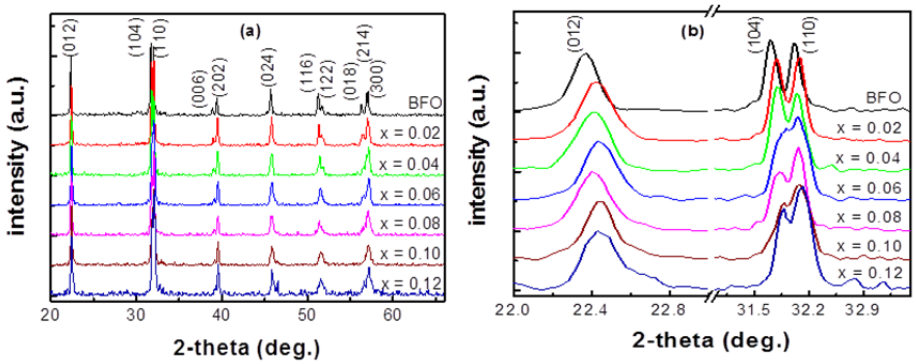

Figure 1. (a) X-ray diffraction diagrams of $BiFeO_3$ and $Bi_{1-x}Sm_xFe_{0.97}Mn_{0.03}O_3$ (x = 0.02, 0.04, 0.06, 0.08, 0.10, and 0.12) materials; (b) Comparison of the positions of the (012), (104), and (110) peaks.

Table 1. Crystal lattice parameters and average crystal size of $BiFeO_3$ and $Bi_{1-x}Sm_xFe_{0.97}Mn_{0.03}O_3$ (x = 0.02, 0.04, 0.06, 0.08, 0.10, and 0.12) samples.

Samples	a (nm)	c (nm)	L_{XRD} (nm)
BFO	0.5584	1.3867	60
x = 0.02	0.5575	1.3819	51
x = 0.04	0.5577	1.3819	49
x = 0.06	0.5576	1.3817	49
x = 0.08	0.5578	1.3833	47
x = 0.10	0.5566	1.3754	43
x = 0.12	0.5563	1.3752	40

3.2. Raman scattering spectra

Raman scattering spectra of BFO and $Bi_{1-x}Sm_xFe_{0.97}Mn_{0.03}O_3$ (x = 0.02, 0.04, 0.06, 0.08, 0.10, and 0.12) materials, as shown in Figure 2. According to the group theory, 13 Raman active modes could be expected for the rhombohedral BFO structure with the R_{3C} space group ($\Gamma = 4A_1 + 9E$) [22,23]. However, not all modes could be clearly observed at room temperature. In the analysis of the Raman scattering spectra for all samples, the positions of the Raman active modes for all samples are fitted by the Gaussian function. As one can see in Figure 2, Raman scattering spectra of the BFO sample has A_1-1, A_1-2, A_1-3, E-2, E-3, E-4 modes, whereas Raman scattering spectra of the

(Sm, Mn) co-doped samples have A_1-1, A_1-2, A_1-3, E-2, E-3, E-4 and E-9 modes. When concentration of Sm increases the A_1-1, A_1-2, A_1-3, E-2, E-3, and E-4 modes shift toward the higher frequencies compared to the situation in the BFO sample. Previous studies have also shown that the A_1 modes and the E modes both at low frequencies are characteristic for the Bi–O covalent bonds, while other E modes at high frequencies are characteristic for the Fe-O bonds [24]. The A_1-1, A_1-2, A_1-3, E-2, E-3, and E-4 modes are found characteristic for the Bi-O covalent bonds [13,25], while the E-9 mode is characteristic for the Fe–O bonds [10,26]. So the observed change positions of the E-9 modes shall confirmed that the Mn^{2+} ions are substituted into the Fe-sites, and the change of the positions of the A_1-1, A_1-2, A_1-3, E-2, E-3, and E-4 modes also confirmed Sm^{3+} ions being substituted into the Bi-sites. These results are consistent with the XRD results, which confirmed that Sm^{3+} and Mn^{2+} ions are substituted into the Bi- and the Fe-sites, respectively.

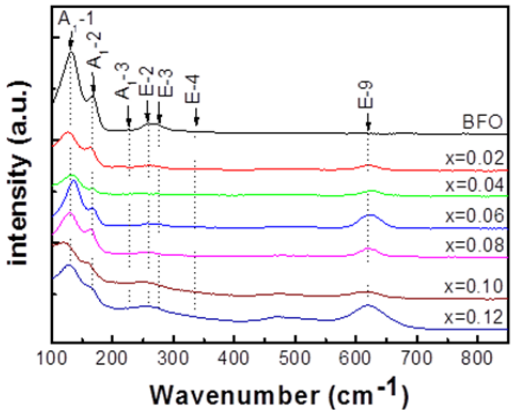

Figure 2. Raman scattering spectra of BFO and $Bi_{1-x}Sm_xFe_{0.97}Mn_{0.03}O_3$ (x = 0.02, 0.04, 0.06, 0.08, 0.10, and 0.12) materials.

3.3. Magnetic properties

Figure 3a shows the magnetic hysteresis loops recorded for the BFO and $Bi_{1-x}Sm_xFe_{0.97}Mn_{0.03}O_3$ (x = 0.02, 0.04, 0.06, 0.08, 0.10, and 0.12) compounds at room temperature. As it is seen in Figure 3a, all samples present a weak ferromagnetic behavior. The BFO sample has a saturation magnetization M_s = 0.015 emu/g and remnant magnetization M_r = 0.007 emu/g. For the (Sm, Mn) co-doped samples, the M_s and M_r values increase up to M_s = 0.04 emu/g and M_r = 0.02 emu/g, as are seen in Figure 3b. These results could be understood from the following consideration. Firstly, the substitution of the Mn^{2+} ions into the Fe-sites creates the exchange interaction between the Mn^{2+} ions with the neighbouring Fe^{3+} ions [27,28] leading to the change of the material's magnetic state from the antiferromagnetic to the ferrimagnetic order; Secondly, there exist double exchange interaction in the Fe^{3+}–O^{2-}–Mn^{2+} chains resulting from the contribution of the 3*d* electrons in the magnetically active Fe/Mn atoms; Thirdly, the substitution of metal ions with another different valence state (i.e. Mn^{2+}) leads to the structural lattice distortion and/or the breakdown of the balance between the antiparallel magnetizations in the sublattice of the Fe^{3+} ions. This can cause the canting of the antiferromagnetic ordering spins and thus enhances the total magnetization of materials [28]; Furthermore, the substitution of the Mn^{2+} ions into the $BiFeO_3$

crystal lattice creates oxygen vacancies and lattice defects, which in turn also contributes to the enhancement of the material's magnetization [29].

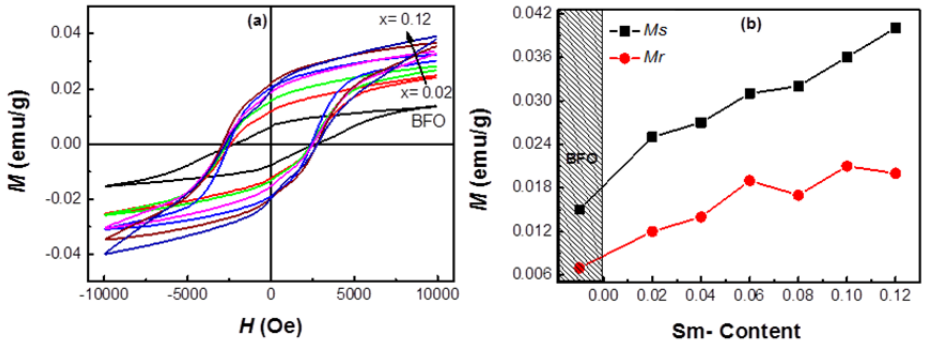

Figure 3. (a) Magnetization hysteresis loops of $BiFeO_3$ and $Bi_{1-x}Sm_xFe_{0.97}Mn_{0.03}O_3$ (x = 0.02, 0.04, 0.06, 0.08, 0.10, and 0.12) materials; (b) The M_s and M_r values depend on concentration of Sm.

3.4. Ferroelectric properties

Figure 4a shows the room temperature polarization as a function of applied-electric fields of BFO and (Sm, Mn) co-doped samples. It is clear that all the samples show ferroelectric behavior. The ferroelectric properties are clearly improved in (Sm, Mn) co-doped samples compared to that of the BFO sample. The saturation polarization (P_s) and remnant polarization (P_r) values of BFO and (Sm, Mn) co-doped samples, as shown in Figure 4b. For (Sm, Mn) co-doped samples show the P_s and P_r values, indicating the best improvement of ferroelectric properties of BFO with (Sm, Mn) co-doping. This observation can be explained as the substitution of Sm into the Bi-sites, leading to modification of the Bi/Sm–O bonding. On the hand, the substitution of Mn into Fe-sites created oxygen vacancies and changes the FeO_6 octahedron, leading to enhancement of P_s and P_r.

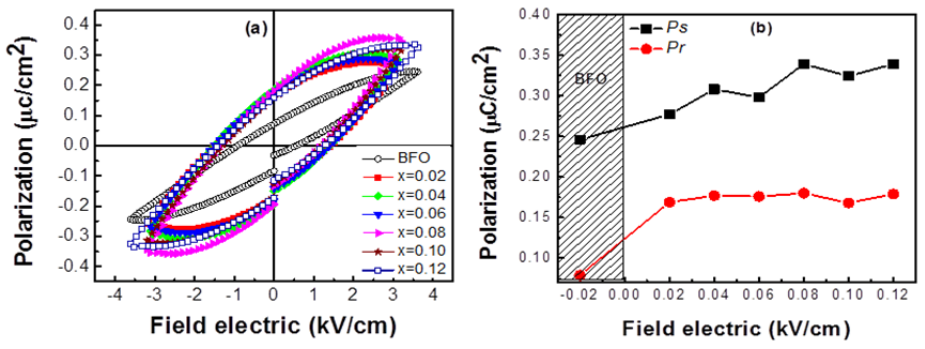

Figure 4. (a) Polarization electric hysteresis loops of $BiFeO_3$ and $Bi_{1-x}Sm_xFe_{0.97}Mn_{0.03}O_3$ (x = 0.02, 0.04, 0.06, 0.08, 0.10, and 0.12) materials; (b) The P_s and P_r values depend on concentration of Sm.

3.5. Complex impedance spectra

Figure 5 shows complex impedance spectra of the $BiFeO_3$ and $Bi_{1-x}Sm_xFe_{0.97}Mn_{0.03}O_3$ (x = 0.02, 0.06, and 0.08) materials. The complex impedance spectra of materials are known to consist of the various contributions from intra- and inter-grains, grain boundaries, and the electrode interfaces. The complex impedance spectra in term of the Cole-Cole plot are presented in successive semicircles indicating the imaginary part vs. the real part in the complex plane. A high frequency semicircles originate from intragrain contributions, a semicircle in the intermediate frequency provides information on the contributions from the grain boundaries, whereas the low frequency semicircle associates to the ion and electron transfer at the contact interface between the sample and the measuring electrode [12,30,31]. Impedance spectra are determined by the frequency range of the measurements, but all these contributions may not be ruled out. Some previous studies also showed the distinction between the intra and the inter-grain contributions which are related to the defects in ferroelectric materials [32,33]. The complex impedance spectra thus can provide reliable information on the dielectric properties of materials. In our work, for all samples, the simulated curves agree quite well with the experimental ones. As it is seen in Figure 5, the impedance spectra of the BFO and (Sm, Mn) co-doping samples consist of a semicircle at the high frequency region, toward zero in the complex plane presenting the intragrain contribution and a semicircle at the intermediate frequency, untoward zero in the complex plane presenting the grain boundaries. However, due to limited measurement frequency range, the contribution of the electrode interface to the impedance could not be fairly detected in all the investigate samples. These presented results provide, thus, just some preliminary information pointing out significant modification of the dielectric properties of the (Sm, Mn) co-doped $BiFeO_3$ materials. Which is consistent with results of the hysteresis loop measurement showed the ferroelectric properties of (Sm, Mn) co-doping samples was improved to compared with that of BFO sample.

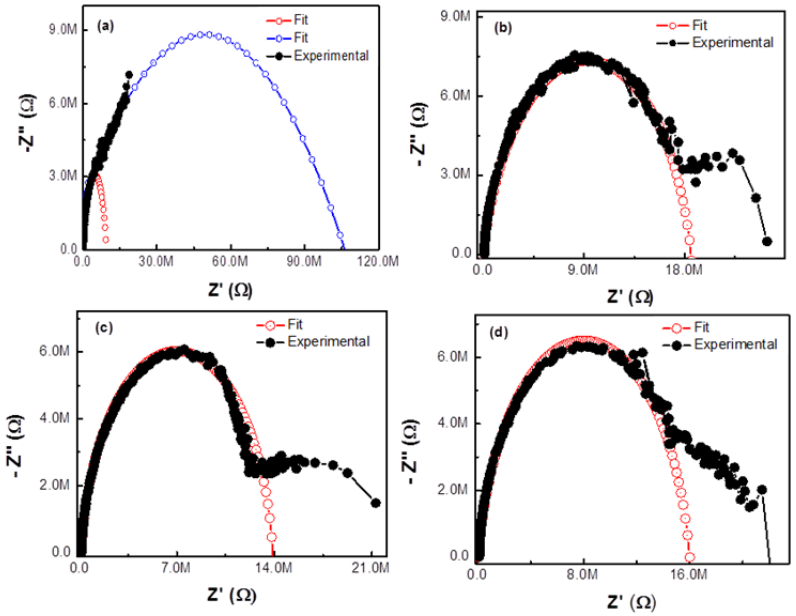

Figure 5. Impedance spectra of $BiFeO_3$ and $Bi_{1-x}Sm_xFe_{0.97}Mn_{0.03}O_3$ samples: (a) $BiFeO_3$; (b) x = 0.02; (c) x = 0.06; (d) x = 0.08.

4. Conclusion

In summary, $BiFeO_3$ and $Bi_{1-x}Sm_xFe_{0.97}Mn_{0.03}O_3$ (x = 0.02, 0.04, 0.06, 0.08, 0.10, and 0.12) materials have been successfully fabricated by citrate method. All samples crystallize in rhombohedral structure of $BiFeO_3$ materials. Crystal lattice parameters and average crystallite size of (Sm, Mn) co-doping samples decreased gradually compared to those of $BiFeO_3$ sample. X-ray diffraction patterns and Raman scattering spectra confirmed the successful substitution of Sm^{3+} and Mn^{2+} ions into Bi- and Fe-sites, respectively, which affected obviously to magnetic and ferroelectric properties of $BiFeO_3$ host materials. Magnetic and ferroelectric properties of (Sm, Mn) co-doping samples enhanced to compared with those of $BiFeO_3$ materials.

Acknowledgements

This work has been supported by the Ministry of Education and Training of Vietnam (Code B2018-MDA-02-CtrVL).

Conflict of interests

The authors declare no conflicts of interests.

References

1. Eerenstein W, Mathur ND, Scott JF (2006) Multiferroic and magnetoelectric materials. *Nature* 442: 759–765.
2. Ederer C, Spaldin NA (2005) Weak ferromagnetism and magnetoelectric coupling in bismuth ferrite. *Phys Rev B* 71: 060401(R).
3. Ravindran P, Vidya R, Kjekshus A, et al. (2006) Theoretical investigation of magnetoelectric behavior in $BiFeO_3$. *Phys Rev B* 74: 224412.
4. Cheong SW, Mostovoy M (2007) Multiferroics: a magnetic twist for ferroelectricity. *Nat Mater* 6: 13–20.
5. Kumarn M, Sati PC, Chhoker S, et al. (2015) Electron spin resonance studies and improved magnetic properties of Gd substituted $BiFeO_3$ ceramics. *Ceram Int* 41: 777–786.
6. Zhang X, Sui Y, Wang X, et al. (2010) Effect of Eu substitution on the crystal structure and multiferroic properties of $BiFeO_3$. *J Alloy Compd* 507: 157–161.
7. Pradhan SK, Das J, Rout PP, et al. (2010) Effect of holmium substitution for the improvement of multiferroic properties of $BiFeO_3$. *J Phys Chem Solids* 71: 1557–1564.
8. Naganuma H, Miura J, Okamura S (2008) Ferroelectric, electrical and magnetic properties of Cr, Mn, Co, Ni, Cu added polycrystalline $BiFeO_3$ films. *Appl Phys Lett* 93: 052901.
9. Dai YR, Xun Q, Zheng X, et al. (2012) Magnetic properties of Ni-substituted $BiFeO_3$. *Physica B* 407: 560–563.
10. Dong G, Tan G, Luo Y, et al. (2014) Optimization of the multiferroic $BiFeO_3$ thin films by divalent ion (Mn, Ni) co-doping at B-sites. *Mater Lett* 118: 31–33.
11. Thang Dv, Hung NM, Khang NC, et al. (2017) Structural, magnetic and electric properties of Nd and Ni co-doped $BiFeO_3$ materials. *AIMS Mater Sci* 4: 982–990.

12. Thang DV, Hung NM, Khang NC, et al. (2019) Structural, electrical, and magnetic properties of $Bi_{0.90}Nd_{0.10}Fe_{0.98}TM_{0.02}O_3$ (TM = Mn, Co, Ni, and Cu) materials. *IEEE Magn Lett* 10: 1–5.
13. Yan X, Tan G, Liu W, et al. (2015) Structural, electric and magnetic properties of Dy and Mn co-doped $BiFeO_3$ thin film. *Ceram Int* 41: 3202–3207.
14. Chakrabarti K, Das K, Sarkar B, et al. (2012) Enhanced magnetic and dielectric properties of Eu and Co co-doped $BiFeO_3$ nanoparticles. *Appl Phys Lett* 101: 042401.
15. Zhang X, Zhang C, Ran N (2016) Tailoring the magnetic and optical characteristics of $BiFeO_3$ ceramics by doping with La and Co. *Mater Lett* 179: 186–189.
16. Ye W, Tan G, Dong G, et al. (2015) Improved multiferroic properties in (Ho, Mn) co-doped BiFeO3 thin films prepared by chemical solution deposition. *Ceram Int* 41: 4668–4674.
17. Kumar A, Sharma P, Yang W, et al. (2016) Effect of La and Ni substitution on structure, dielectric and ferroelectric properties of $BiFeO_3$ ceramics. *Ceram Int* 42: 14805–14812.
18. Yun Q, Xing W, Chen J, et al. (2015) Effect of Ho and Mn co-doping on structural, ferroelectric and ferromagnetic properties of $BiFeO_3$ thin films. *Thin Solid Films* 584: 103–107.
19. Park JS, Yoo YJ, Hwang JS, et al. (2014) Enhanced ferromagnetic properties in Ho and Ni co-doped $BiFeO_3$ ceramics. *J Appl Phys* 115: 013904.
20. Rajput SS, Katoch R, Sahoo KK, et al. (2015) Enhanced electrical insulation and ferroelectricity in La and Ni co-doped $BiFeO_3$ thin film. *J Alloy Compd* 621: 339–344.
21. Xu X, Guoqiang T, Huijun R, et al. (2013) Structural, electric and multiferroic properties of Sm-doped $BiFeO_3$ thin films prepared by the citrate process. *Ceram Int* 39: 6223–6228.
22. Hermet P, Goffinet M, Kreisel J, et al. (2007) Raman and infrared spectra of multiferroic bismuth ferrite from first principles. *Phys Rev B* 75: 220102.
23. Luo L, Wei W, Yuan X, et al. (2012) Multiferroic properties of Y-doped $BiFeO_3$. *J Alloy Compd* 540: 36–38.
24. Yuan GL, Or SW, Chan HL (2007) Raman scattering spectra and ferroelectric properties of $Bi_{1-x}Nd_xFeO_3$ (x = 0–0.2) multiferroic ceramics. *J Appl Phys* 101: 064101.
25. Gautam A, Singh K, Sen K, et al. (2011) Crystal structure and magnetic property of Nd doped $BiFeO_3$ nanocrytallites. *Mater Lett* 65: 591–594.
26. Arora M, Sati PC, Chauhan S, et al. (2014) Structural, magnetic and optical properties of Ho–Co codoped $BiFeO_3$ nanoparticles. *Mater Lett* 132: 327–330.
27. Yu L, Deng H, Zhou W, et al. (2016) Effects of (Sm, Mn and Ni) co-doping on structural, optical and magnetic properties of $BiFeO_3$ thin films fabricated by a citrate technique. *Mater Lett* 170: 85–88.
28. Rajan PI, Mahalakshmi S, Chandra S (2017) Establishment of half-metallicity, ferrimagnetic ordering and double exchange interactions in Ni-doped $BiFeO_3$—A first-principles study. *Comp Mater Sci* 130: 84–90.
29. Xue X, Tan G, Dong G, et al. (2014) Studies on structural, electrical and optical properties of multiferroic (Ag, Ni and In) codoped Bi0.9Nd0.1FeO3 thin films. Appl Surf Sci 292: 702–709.
30. Thang DV, Van Minh N (2016) Magnetic properties and impedance spectroscopic studies of multiferroic $Bi_{1-x}Nd_xFeO_3$ materials. *J Magn* 21: 29–34.
31. Yao Y, Tao T, Liang B, et al. (2019) Pyroelectric properties and AC impedance study of bismuth ferrite ($BiFeO_3$) ceramics. *Ceram Int* 45: 1308–1313.
32. Wang X, Liu J, Liang P, et al. (2018) Higher curie temperature and enhanced piezoelectrical properties in $(Ba_{0.85}Ca_{0.15-x}Pb_x)(Zr_{0.1}Ti_{0.90-y}Sn_y)O_3$ Ceramics. *J Electron Mater* 47: 6121–6127.

33. Sahoo S, Hajra S, De M, et al. (2018) Processing, dielectric and impedance spectroscopy of lead free $BaTiO_3$–$BiFeO_3$–$CaSnO_3$. *J Alloy Compd* 766: 25–32.

AIMS Press